Preprint

UCRL-JC- 154476

Evaluation of the Impact of CO_2, Co-contaminant Gas, Aqueous Fluid and Reservoir Rock Interactions on the Geologic Sequestration of CO_2

Kevin G. Knauss
James W. Johnson
Carl I. Steefel
Environmental Science Division
Lawrence Livermore National Laboratory
Livermore, CA 94550 USA

This article was submitted to
Chemical Geology

June 2003

Evaluation of the impact of CO_2, co-contaminant gas, aqueous fluid and reservoir rock interactions on the geologic sequestration of CO_2

Kevin G. Knauss, James W. Johnson and Carl I. Steefel

Earth Sciences Division

Lawrence Livermore National Laboratory

Livermore, CA 94550, USA

(knauss@llnl.gov 925-422-1372 (phone) 925-422-3925 (fax))

Submitted to *Chemical Geology* 6/03

Revised manuscript submitted 5/04

ABSTRACT

Lowering the costs of front-end processes (e.g., separation) in the geologic sequestration of CO_2 can dramatically lower the overall costs. One possible approach is to sequester less-pure CO_2 waste streams that are less expensive or require less energy to separate from flue gas or a coal gasification process, etc. The objective of this research is to evaluate the impacts of CO_2 itself, as well as an impure CO_2 waste stream, on geologic sequestration using reaction progress models, reactive transport simulators and analogous reactive transport experiments run in a plug flow reactor. Specifically, we are investigating the potential for co-injecting the SO_x, NO_x, and H_2S present in coal-fired waste streams along with the CO_2.

We present here the results of reactive transport simulations made to investigate the long-term impact of dissolved CO_2, H_2S and SO_2 on carbon sequestration in the Frio Fm., TX. The results suggest that addition of relatively large amounts of H_2S to a CO_2 injection should not adversely impact injectivity or sequestration compared to the injection of CO_2 alone. The co-injection of SO_2, however, could produce significantly different results, if conditions are such that SO_2 can oxidize to sulfate. In the long-term the simulations suggest that carbonate mineral formation can sequester a significant fraction of the injected carbon through the formation of calcite, magnesite and dawsonite.

Keywords: reactive transport modeling; geologic CO_2 sequestration; rock-water interaction; Frio Fm.

INTRODUCTION

The costs of separation and compression of CO_2 from point sources, e.g., coal-fired power plants, have been estimated to account for 75% of the total cost of a geologic sequestration process. Obviously, lowering the costs of the front end processes can dramatically lower the overall costs. One approach to lower cost is to permit a waste stream to be less than pure CO_2. The evaluation of the additional impact of this impure CO_2 waste stream on geologic sequestration is the goal of this project.

The three primary candidate formation/reservoir types suggested for geologic sequestration: oil and gas reservoirs, coal beds and deep saline formations, all contain aqueous phases. Oil fields under active EOR (enhanced oil recovery) may have additional (foreign) water used in flooding. Although CO_2 injected as part of a geologic sequestration effort may initially behave as an immiscible phase, it can chemically react with water to form carbonic acid and then further react with or form mineral phases once it has dissociated into bicarbonate or carbonate aqueous species. This interaction of CO_2 with water is the ultimate basis for the geologic sequestration processes of solubility trapping (as carbonate aqueous species) and mineral trapping (as carbonate minerals). It is essential, therefore, to have a good understanding of the effect of CO_2 injection on aqueous and mineral phase chemistries, as well as the physics of flow involving immiscible fluids.

Only a handful of directly relevant experiments and supporting geochemical modeling have been done to date (e.g., (Czernichowski-Lauriol et al., 1996;

Gunter et al., 1997; Kaszuba et al., 2003; Sass et al., 2000). These preliminary studies focused on the impact of elevated CO_2 fugacity on mineral dissolution and precipitation, as well as the impact on brine chemistry. They drew some general inferences from their results relating to dissolution of carbonate cements and the potential for both carbonate and silicate mineral formation with the accompanying impact on porosity/permeability. These inferences relate directly to injectivity issues, as well as to the long term performance of geologic sequestration due to CO_2 solubility and mineral trapping. However, these early studies did not assess the direct or indirect impact of waste stream contaminants (NO_x, SO_x, H_2S, etc.) on injectivity and long term performance, nor did they explicitly evaluate the impact of transport processes. This evaluation will also require the laboratory experimental validation of the reactive transport simulators themselves. More recently, modeling efforts have begun to investigate the impact of waste stream contaminants (Gunter et al., 2000; Knauss et al., 2001). These impacts must be evaluated to optimize front end processes (separation and compression) and lower costs.

Our own recent work (Knauss et al., 2002) began to address not only the impact of the waste gases, but also the impact of transport processes. Most recently we have begun to validate our simulator using reactive transport experiments conducted in a specially designed plug flow reactor (PFR). In the preliminary simulations we used simplified, generic reservoir rocks defined as follows. The feldspathic sandstone reservoir consisted of: 88.5% quartz, 9% K-feldspar, 1% calcite, 0.5% siderite, 0.5% pyrite and 0.5% muscovite. The siderite was added

to the mix as a proxy for solid solution of Fe in the calcite. The muscovite was added as a proxy for all clay-like phases, e.g., illite. The carbonate reservoir consisted of: 49.25% calcite, 49.25% dolomite, 0.75% siderite and 0.75% pyrite. Both generic reservoirs were assumed to have 33% porosity. The simplified brine composition consisted of 0.7 m NaCl. Although these generic models do resemble the majority of reservoirs likely to be encountered, it is an important next step to use real measurements of both fluids and rocks from real reservoirs. An example of such a study is presented here.

Ultimately, we need to identify and quantify the impact of waste stream contaminants (NO_x, SO_x, H_2S, etc.) on injectivity. This will permit definition in composition space of allowable concentrations of contaminants (i.e., upper limits) and provide criteria for injection optimization. We also need to identify and quantify the post-injection (longer term) chemical behavior of CO_2 in the presence of contaminants. This will permit evaluation and prediction of the long term performance of geologic sequestration of CO_2 as a climate control process.

APPROACH

Coupling a chemical model with simplified fluid flow using the reactive transport code CRUNCH (Steefel, 2001; Steefel and MacQuarrie, 1996), we have simulated the results of injection of $CO_2 \pm$ contaminants into a specific heterogeneous rock formation and have calculated the mineralogical changes along the flow path. The reactive transport approach is essential for calculating the spatial distribution of porosity change, because reaction products tend to be

distributed along a flow path. We also recognize the need to use both natural analogues (e.g., the CO_2 trapped at the Bravo Dome, (Pearce et al., 1995) and ideal physical models (e.g., lab experiments using plug flow reactors, (Johnson et al., 1998) to benchmark results obtained using reactive transport simulators.

The reactive transport simulator CRUNCH is a computer software package for simulating multicomponent, multi-dimensional reactive transport in porous media. The features of the code include:

- simulation of advective, dispersive, and diffusive transport in up to two dimensions using the global implicit (*GIMRT*) option or three dimensions using time-splitting of transport and reaction (*OS3D*);
- non-isothermal transport and reaction;
- unsaturated transport with gas-aqueous phase exchange;
- multicomponent aqueous complexation;
- kinetically-controlled mineral precipitation and dissolution;
- multicomponent ion exchange on multiple sites;
- multicomponent surface complexation on multiple sites with or without an electrostatic correction based on the double layer model (Dzombak and Morel, 1990). Site densities are linked to mineral concentrations which may evolve;
- microbially-mediated reactions based on Monod-type formulations;
- radioactive decay chains;
- advective transport of solid phases to simulate erosion or burial;
- multicomponent diffusion with an electrochemical migration term to correct for electroneutrality where diffusion coefficients of charged species differ;
- multiple options (equilibration with a gas or mineral phase, total concentration, fixed activity) for initialization of boundary and initial conditions;
- automatic read of a reformatted version of the EQ3/EQ6 database augmented with a kinetic database (WOLERY et al., 1990).

The simulation is described in detail in the next section but, in brief, we have first equilibrated the model reservoir fluid with contaminant gas(es) and then flowed

the aqueous fluid phase through a model reservoir porous media under isothermal (T = 64°C), isobaric (P_{tot} = 100b) fully saturated conditions. The flux of injected aqueous fluid was volumetrically equivalent to the amount of CO_2 planned to be injected during a pilot project in the Frio Fm., TX.

MODEL DEFINITION

Our model was constructed using reservoir fluid and rock data from wells completed in the Frio Fm. in Texas. This unit is the proposed site for a CO_2 sequestration pilot project (Hovorka et al., 2002). The model mineralogy and modal abundances, based on an average of 12 petrographic and XRD analysis for Frio Fm. sand samples from well Merisol WDW No. 319, are shown in Table 1, that also contains calculated (geometric) mineral specific surface areas (SSA), assuming 200 μ spherical grains with no roughness. SEM examination of the sand revealed well rounded grains of this average diameter. The specific surface area calculation is made using this radius and the molar volume and molecular weight of each mineral. The edge factor provides an adjustment (multiplier) made to this calculated SSA based on the apparent increase in mineral surface area and reactivity due to edges in sheet silicate minerals (Nagy et al., 1999).

The model reservoir fluid composition (Table 2) is based on water samples taken from a nearby well (GNI WDW-169) completed in the Frio sand. Because the fluid analyses were incomplete (they failed to analyze for K, Al, Si or O_2), as a starting point for the reservoir fluid model composition we assumed that these missing elements were controlled by mineral equilibria (illite, kaolinite, quartz and

pyrite, respectively) and then used CRUNCH to react a very slowly moving reservoir fluid of this composition with the rock sufficiently long (2000 years) until a nearly steady-state fluid composition was achieved. In this calculation the initial chemical state of the aqueous system is determined by the assumed mineral equilibria only for the missing elements and all other element concentrations are based on the measured values, but after the initialization the model runs with full reaction kinetics. The purpose of this initial simulation is to arrive at a model formation fluid composition that represents a nearly steady state condition in the reservoir for the specified reservoir T and P conditions and mineral composition. It is not at equilibrium, but nearly so. The redox state is initially set by the measured Fe^{++} and the assumed equilibria with pyrite. The redox state may then evolve as reaction progress advances. This calculation also allowed us to identify the secondary minerals that could potentially form in this system (anhydrite, barite, chalcedony, dawsonite, magnesite, siderite and strontianite). In Table 2 the total molal concentrations are given in terms of the basis species. The code does a speciation calculation of individual species concentrations for each element, including the redox active elements (e.g., Fe^{++}/Fe^{+++}, $HS^{-}/SO4^{--}$, etc.), at each time step in the simulation.

Note that in the subsequent CRUNCH simulations of CO_2 injection the code initializes the chemical system before CO_2 injection using this model composition for the fluid and calculates in situ pH by charge balance. The calculated reservoir fluid pre-injection pH is 6.74. This agrees reasonably well with the measured well pH of 6.85.

Because the reservoir fluids become acidic upon CO_2 injection, we use kinetic rate laws that explicitly account for acid catalysis of mineral dissolution. The rate law that we use in CRUNCH has a transition-state-theory (Laidler, 1987) like, "TST-like", formulation that may be written as:

$$r_m = A_m k_m \exp\left(-E_a/RT\right)\prod_{i=1}^{N} a_i^n\left(1 - Q/K\right)$$

where: r_m = rate of dissolution or growth, A_m = mineral surface area, k_m = intrinsic rate constant, E_a = activation energy, $\prod_{i=1}^{N} a_i^n$ is a product term accounting for kinetic inhibition or catalysis by any species in solution with empirical reaction order n, Q = ion activity product and K = the corresponding equilibrium product. In this work we only account for the effect of H^+ on rate, i.e., there is a reaction order value given in Table 2 with respect to the activity of H only. Note that in this formulation the same rate law is being used to describe both dissolution and growth according to the principle of microscopic reversibility (by simply running it forwards or backwards) and this is, most certainly, an empirical approximation anywhere in free energy space removed from equilibrium. Currently, we are conducting simulator validation experiments using our PFR to determine the most appropriate formulation.

Because the reservoir is at an elevated temperature (and we are especially interested in kinetics), we use Helgeson's extended Debye-Huckel formalism (B-dot) for calculating activity coefficients for aqueous species(Helgeson and Kirkham, 1974). Note that the calculated ionic strength in the model fluid at

reservoir conditions is 1.7 molal, which is slightly beyond the range in ionic strength over which this formalism is typically applied, even though the fitting Helgeson did spanned the range 25-300°C and 0-3 molal NaCl. Unfortunately, high temperature Pitzer parameters (Pitzer, 1973), which explicitly correct for high ionic strength solutions, are unavailable for many of the species of interest in this calculation, hence the compromise: we are well within the temperature range where B-bot works well, but slightly outside the ionic strength range over which it is typically applied. Activity coefficients for neutral aqueous species are assumed to be 1. However, in the case of CO_2 itself, we have calculated the fugacity coefficient separately, so that the injection pressure of CO_2 (100b) is converted to the actual fugacity of CO_2 (84.3b) at reservoir conditions. The species CO_2(aq) like all neutral aqueous species is assumed to have an activity coefficient of 1 when calculating solubility and it is assumed to be in instantaneous equilibrium with CO_2(g).

The kinetic parameters that we use in the model are shown in Table 3. In this table we include the separate intrinsic rate constant (k), the activation energy (E_a), and the reaction order (n) for each mechanism (acid catalyzed and no catalysis). At any pH the total rate is the sum of the rates via each mechanism. The thermodynamic parameters used to calculate Q and K are taken for the most part from the EQ3/6 database (Wolery et al., 1990), which in turn is derived mostly from SUPCRT data (Johnson et al., 1992).

To track the position of the front, in the simulation we include a perfectly conservative tracer. It may be assumed to move with the water and is included in all subsequent fluid chemistry plots.

In these preliminary simulations we have set up a very simple1D, radially symmetric model for injection. We used an analytical expression to calculate a radial Darcy flow field that closely approximates the flow field (and resulting observation well breakthrough times) that were generated from TOUGH2 (Pruess, 2002) transport-only modeling of CO_2 injection into the Frio Fm. sand (Doughty, 2002). The expression we used is:

$$\mathbf{V(x) = Q/(2\pi x h \varphi S_g \rho)}$$

where: V(x) = Darcy flux at x, x = radial distance, Q = CO_2 injection rate (250T/d), h = cylinder height of injection interval, φ = porosity (30%), S_g = residual gas saturation behind front (0.55), and ρ = density of CO_2 at T&P (565 kg/m^3 at 64°C and 150b total CO_2 pressure). For our simulation this results in a velocity field falling off rapidly from very high Darcy velocities 1 m from the well bore (4279 $m^3m^{-2}y^{-1}$) to much lower values 1 km from the well bore (4 $m^3m^{-2}y^{-1}$). Under injection conditions the CO_2 fugacity is 84.3b.

Because our primary interest is in the rock/water interaction arising from the acid created by dissolving CO_2 and other waste gases, we simplified the simulation by injecting the volume equivalent amount (i.e., using the Darcy flux radial flow field calculated above) of the reservoir fluid equilibrated with the appropriate waste gas fugacities. In the CO_2 only case, this is 84.3b; for the CO_2 + H_2S case we

added 10b of H_2S; and for the CO_2 + SO_2 case we added 10^{-6}b of SO_2. This is the amount of SO_2 which results in a fluid pH of 1, when equilibrated with the reservoir fluid, and permitting the SO_2 to be oxidized to sulfate, if thermodynamically able to do so. Note that, although the solution O_2(aq) concentration is insufficient to oxidize very much SO_2, there are at least two other thermodynamically favored oxidants present in abundance: pyrite or water itself. In the first case the reductive dissolution of pyrite involves conversion of the mineral persulfide S^{-1} to aqueous S^{-2} coupled to the aqueous oxidation of S^{+4} to S^{+6} sulfate and H^+. The reaction is:

$$FeS_2 + SO_2(g) + 2H_2O = Fe^{++} + 2S^{--} + 4H^+ + SO_4^{--}$$

In the second case water can be reduced to H_2(aq) to produce sulfate and associated H^+. The reaction then is:

$$SO_2(g) + 2H_2O = H_2(g) + 2H+ + SO_4^{--}$$

Given the abundance of potential oxidants, the assumption that the SO_2 will eventually be oxidized to sulfate is not an unreasonable one based on thermodynamics.

To simulate conditions associated with a long term sequestration effort, we continued the injection phase for 5y under the radial flow field just described and then instantaneously switched to a much slower linear flow field (a Darcy flow of 0.15m/y) of the starting composition reservoir fluid (i.e., acid gas free). This would approximate the return to slow regional flow after injection stops and these new conditions were simulated for an additional 95y. We simulated the reactive

transport over a 1km domain with 164 cells progressing in size from 1m near the injection well to 10m further out into the domain. We show the model schematically in Fig. 1.

RESULTS & DISCUSSION

In Fig. 2 we plot the aqueous phase concentrations of the dominant species produced from the injected gases, as well as the tracer, at the end of the injection period. In Fig. 3 we plot the distribution of C-bearing minerals at the same time point. Because pH is the master variable in these chemical systems, largely dictating aqueous speciation and mineral dissolution and/or growth, we plot it as the right-hand axis on all plots.

A number of points can be made here, initially dealing with the CO_2 only case as a baseline for discussion. At the end of the injection period (5y) the tracer has progressed some 750 m into the domain, although the CO_2(aq) front propagates at a slower velocity due to rock/water interactions, etc. The incoming fluid (the fluid contained in the first cell in the domain) at this point in time has a pH of 3.2 (fixed by the CO_2 fugacity), because all the calcite originally present has been consumed (see Fig. 3). As a result, there is no longer pH buffering near the injection point. The calcite is completely consumed over the first 75 m, where the pH over this interval is below that required for calcite stability (approx. pH 4.6). At about 75 m there is an abrupt pH front where it rises above the point of calcite stability. Between about 75m – 300m, an interval where the pH permits calcite stability, the formation original calcite still remains and is growing, consuming the

excess Ca^{+2} liberated upstream by dissolution of both calcite and labradorite, where pH is too low for calcite to be stable.

The addition of H_2S to the waste stream doesn't have a large effect on the rock/water interaction. The SO_2, however, does make a significant difference due to the lower pH created. Note the different (larger) pH scale for this plot. By the end of injection the incoming fluid has a pH of 1. Also, the distribution of aqueous S-species differs markedly (SO_4^{--} vs. $H_2S(aq)$), accompanied by the formation of anhydrite over the first 200m of the domain in the case of SO_2 injection.

In Fig. 3 it is clear that new (additional) carbonate minerals are forming. Although some of the calcite is simply being mobilized and moved downstream, where it can reprecipitate under favorable pH conditions, the formation of dawsonite and magnesite represent new C sinks. Note how the distribution of the carbonate minerals in space displays a chromatographic effect, reflecting the pH distribution, and mapping out the pH stability fields for each mineral.

Although the formation of calcite and magnesite in the simulations involves the familiar carbonate mineral forming reactions, dawsonite represents the formation of a mixed hydroxy-carbonate mineral, as shown in the following possible reaction starting from a calcic plagioclase similar to that in the Frio:

$$2NaCa_{0.5}Al_2Si_2O_8 + 2H_2O + 3CO_2 = 2NaAlCO_3(OH)_2 + 4SiO_2 + CaCO_3 + Al_2O_3$$

For the following discussion we will simplify the reaction to start from the plagioclase endmember, albite:

$$NaAlSi_3O_8 + H_2O + CO_2 = NaAlCO_3(OH)_2 + 3SiO_2$$

At the type locality dawsonite is inferred to have an early hydrothermal origin as a primary mineral (Stevenson and Stevenson, 1965), and it could have formed following the above reaction under likely hydrothermal conditions. However, worldwide it also occurs as an authigenic mineral. In these locations (Olduvai Gorge, the Green River Fm. of Colorado, and the Sydney Basin of New South Wales) it is thought to have formed under alkaline conditions and at much lower temperatures (30 - 75°C) (Baker et al., 1995; Goldbery and Loughnan, 1970; Goldbery and Loughnan, 1977; Smith and Milton, 1966). In these locations it is commonly associated with zeolites and evaporite minerals indicating a pH above neutral. Under these alkaline conditions a more likely reaction is:

$$NaAlSi_3O_8 + OH^- + CO_3^{--} + 5H_2O = NaAlCO_3(OH)_2 + 3H_3SiO_4^-$$

This raises an interesting question concerning the kinetics of dawsonite formation. Experimental work done to date on dawsonite synthesis strongly suggests that an alkaline environment (possibly highly alkaline) is necessary for its formation (Chesworth, 1971; Jackson et al., 1972). However, nothing is known about growth kinetics under the acid pH condition expected to develop during a CO_2 injection. For this work we have simply made the arbitrary assumption that the rate is mid-way between calcite and magnesite. Recently, reaction progress calculations (no kinetics) for a natural analogue site suggest that dawsonite could form at pH as low as pH 6, but this still leaves the kinetics of formation as an open question. Indeed, these authors (Moore et al., 2003) state that field evidence suggests that dawsonite forms under a narrow range of geochemical

conditions, implying that it may not be a significant carbon sink, although we note that the solution composition for the natural analogue calculations is grossly different from those appropriate for the Frio Fm., or for most other potential reservoir sites.

Because existing thermodynamic data suggest that dawsonite could be an important sequestering mineral for C in the Frio Fm. and most other sandstone reservoirs, it is imperative that the growth kinetics of this mineral be determined under the acidic conditions produced during CO_2 injection and in formation waters of more typical composition. There are no available kinetic rate measurements for either dissolution or growth. However, we did several "sensitivity" simulations in which the rate constant for dawsonite was increased to be equal to calcite, decreased to be equal to magnesite and even slowed to the point of never forming. Although the results obviously differ in specific detail, the absence of dawsonite simply results in an increased formation of calcite and magnesite in each simulation.

Note that the thermodynamic data for dawsonite (Ferrante et al., 1976) includes all the thermodynamic properties needed to make reasonably accurate temperature extrapolations, including the Maier-Kelly heat capacity coefficients. We have confidence that the presence of dawsonite in the simulation results is thermodynamically reasonable. The kinetics of its formation remains an open question.

In Figs. 4 & 5 we show the comparable plots after 95 years of flow under a simulated slow regional flow condition, following the 5 year injection phase.

Based on the return of the tracer peak to the original (low) starting reservoir fluid tracer concentration (see Fig. 4), it is seen that the front has moved less than an additional 50 m in the post-injection time period. However, under these more stagnant flow conditions the fluid chemistry and mineralogy have continued to evolve. Compared to Figs 2 & 3, in Figs 4 & 5 in all 3 cases the pH has risen everywhere throughout the domain, while the CO_2(aq) curves have correspondingly decreased. This is due to continued rock/water interaction dominated by the dissolution of silicate minerals at low pH and the growth of carbonate minerals that consume the liberated metals. As pH increases above approximately 6.5, the aqueous C-speciation is also changing to be dominated by HCO_3^-, rather than CO_2(aq). The H_2S(aq) distribution is only slightly changed, while SO_4^{--} is decreased more noticeably by continued formation of anhydrite.

In Fig 5 it is clear that all 3 carbonate minerals have continued to grow under the slow flow conditions following injection. In fact, the carbonate minerals will continue to grow for a long time period beyond the simulation that we have done. This process forms the basis for the mineral sequestration of C that will occur as the initially immiscible CO_2 phase is gradually dissolved and as the dissolved C then reacts with the metals in solution to form the carbonate minerals: calcite, magnesite and dawsonite.

One way to compare the fate of C in the simulations, case by case, is to approximate the inventory of total C in fluids and the total C in solids over the entire domain, comparing the starting distribution to that after the 100 year simulation. To simplify things we calculate an approximate total solution mass for

each cell by multiplying the molal concentration in that cell by the cell length, i.e., assuming the cell height and width are 1m. In the case of the C in solids, this "concentration" represents the mol C per liter of porous media (i.e., minerals + pore space). The results are contained in Table 4.

After 100 years it can be seen that the CO_2 only and the CO_2 & H_2S cases are virtually identical in terms of the C inventory. In the case of CO_2 & SO_2 more C remains in the fluid and less has been trapped as mineral. This occurs because even after 100 years in the presence of SO_2 the pH remains too low over much of the domain for the carbonate minerals to be stable. However, as more time elapses, the extra C in the fluid will eventually become trapped as mineral carbonate as the acid is neutralized through silicate dissolution. In fact, in the SO_2 case more C will eventually be trapped as mineral carbonate than in the other 2 cases, because additional alkaline earth metals and Al have been released to solution from the dissolution of primary reservoir minerals.

CONCLUDING REMARKS

These preliminary simulations would suggest that even relatively large amounts of co-injected H_2S should not prove problematic for a CO_2 injection process. In the case of SO_2, if conditions allow the S to be oxidized, only minor amounts of this gas could be tolerated, due to the extremely low pH generated. Potential for porosity loss due to the formation of anhydrite will also need to be assessed.

It is important to emphasize here that more fully coupled simulations need to be conducted that allow explicit feedback between porosity/permeability changes

and transport processes, as well as dealing explicitly with the transport of a separate CO_2-rich phase (Johnson et al., 2000). For example, in an actual CO_2 injection process the bulk of the CO_2 injected over the time frame of this simulation would still remain as the free immiscible phase. Dissolved CO_2 would be a significant sink for C (see Table 4), while the amounts of carbonate mineral formed would be a smaller sink, as indicated in Figs. 3 & 5.

As mentioned earlier, the lack of kinetic data concerning dawsonite dissolution or growth rate is a problem. Experimental determination of these rates under likely CO_2 sequestration conditions is urgently needed. It is also critical that we conduct well designed reactive transport experiments to benchmark the simulators that we use. Although our ability to simulate dissolution kinetics appears to be relatively advanced, we have few tests of the simulator's ability to accurately model mineral growth. This is a serious deficiency in the work done to date that will require conducting plug flow reactor experiments that closely mimic conditions in a CO_2 injection process and that may be used for this validation purpose.

ACKNOWLEDGEMENTS

Chris Doughty (LBL) graciously provided simulation results from TOUGH hydrologic model runs and suggested the analytical form for the radial flow field expression. The technical support of Ben Reamed, Natalie Drest, and Amanda B. Reconwith is greatly appreciated. This work was funded as Task A3 in the Geo-Seq project. This work was performed under the auspices of the U.S.

Department of Energy by the University of California, Lawrence Livermore National Laboratory under Contract No. W-7405-Eng-48.

Table 1 – Model Reservoir Formation Rock

Mineral	Composition	Mode (vol %)	SSA* (m^2/g)	Edge factor
Quartz	SiO_2	60.06	0.01133	
K-feldspar	$KAlSi_3O_8$	4.26	0.01173	
Illite/muscovite	$KAl_3Si_3O_{10}(OH)_2$	0.96	0.01060	10x
Calcite	$CaCO_3$	0.71	0.01107	
Kaolinite	$Al_2Si_2O_5(OH)_4$	0.66	0.01156	10x
Chlorite/Mg-clinochlore	$Mg_5Al_2Si_3O_{10}(OH)_8$	0.51	0.01118	10x
Labradorite	$Na_{.8}Ca_{.6}Al_2Si_2O_8$	2.48	0.01087	
Pyrite	FeS_2	0.35	0.00599	

* = For a spherical grain the specific surface area SSA = A*v/V*MW, where A = sphere area, v = molar volume, V = sphere volume and MW = molecular weight.

Table 2 – Model Reservoir Formation Fluid

Species (basis)	Concentration (molality)
Al+++	3.2234×10^{-8}
Ba++	4.3092×10^{-4}
Sr++	1.2490×10^{-3}
Ca++	5.5291×10^{-2}
CO_2(aq)	1.0097×10^{-3}
Fe++	6.4972×10^{-4}
K+	1.0594×10^{-2}
Mg++	1.9001×10^{-2}
Na+	1.7767
SiO_2(aq)	4.0135×10^{-4}
Cl-	1.9394
SO4--	1.0746×10^{-4}
O_2(aq)	4.8417×10^{-63}

Table 3 – Kinetic Data

mineral	log k (mol/m^2*s)	E_a (kcal)	n*	source
Albite	-9.69	14.3	.5	Blum & Stillings (1995)
Albite	-12.0	16.2	0	Blum & Stillings (1995)
Anhydrite	-2.76	7.65	.11	Barton & Wilde (1971); Dove & Czank (1995)
Labradorite	-8.86	15.9	.5	Blum & Stillings (1995)
Labradorite	-12.0	16.2	0	Assume similar to albite
Barite	-7.19	7.65	.11	Dove & Czank (1995)
Calcite	-1.16	4.54	1.0	Alkattan et al. (1998)
Calcite	-6.19	15.0	0	Chou et al. (1989)
Chalcedony	-12.7	16.5	0	Rimstidt & Barnes (1980) - α-cristobalite
Clinochlore	-11.6	15.0	0	Malmstrom et al. (1996)
Dawsonite	-7.00	15.0	0	Assume between calcite and magnesite
K-feldspar	-9.45	12.4	.4	Blum & Stillings (1995)
K-feldspar	-12.0	13.8	0	Blum & Stillings (1995)
Kaolinite	-11.6	15.0	.17	Nagy (1995)
Kaolinite	-13.0	15.0	0	Nagy (1995)
Magnesite	-4.36	4.54	1.0	Chou et al. (1989)
Magnesite	-9.35	15.0	0	Chou et al. (1989)
Muscovite	-11.7	5.26	.4	Knauss & Wolery (1989); Nagy (1995)
Muscovite	-13.0	15.0	0	Knauss & Wolery (1989); Nagy (1995)
Pyrite	-8.00	15.0	0	Steefel (2001)
Quartz	-13.9	20.9	0	Testor et al. (1994)
Siderite	-3.01	5.00	.9	Gautelier et al. (1999) - dolomite
Siderite	-8.90	15.0	0	Steefel (2001)
Strontianite	-3.03	10.0	1	Sonderegger (1976)
Strontianite	-7.35	10.0	0	Sonderegger (1976)

* = applies only to the activity term for H+ in the general rate equation given in text

Table 4 – C Inventory

	Pre-injection	CO_2	$CO_2 + H_2S$	$CO_2 + SO_2$
Fluid (mols)	1.04	186	185	259
Mineral (mols)	190	287	284	228

FIGURE CAPTIONS:

Fig. 1: Schematic of the conceptual model for the simulation. The simulation discretization in space is indicated as sections A through E in the domain, where each section contains the indicated number of nodes of the same size.

Fig. 2: Molal concentrations and pH throughout the domain at the end of the injection phase (5y).

Fig. 3: Volume percent of carbonate minerals throughout the domain at the end of the injection phase (5y).

Fig. 4: Molal concentrations and pH throughout the domain after an additional 95y of slow background flow.

Fig. 5: Volume percent of carbonate minerals throughout the domain after an additional 95y of slow background flow.

FIGURE 1 - SCHEMATIC OF THE CONCEPTUAL MODEL FOR THE SIMULATION.

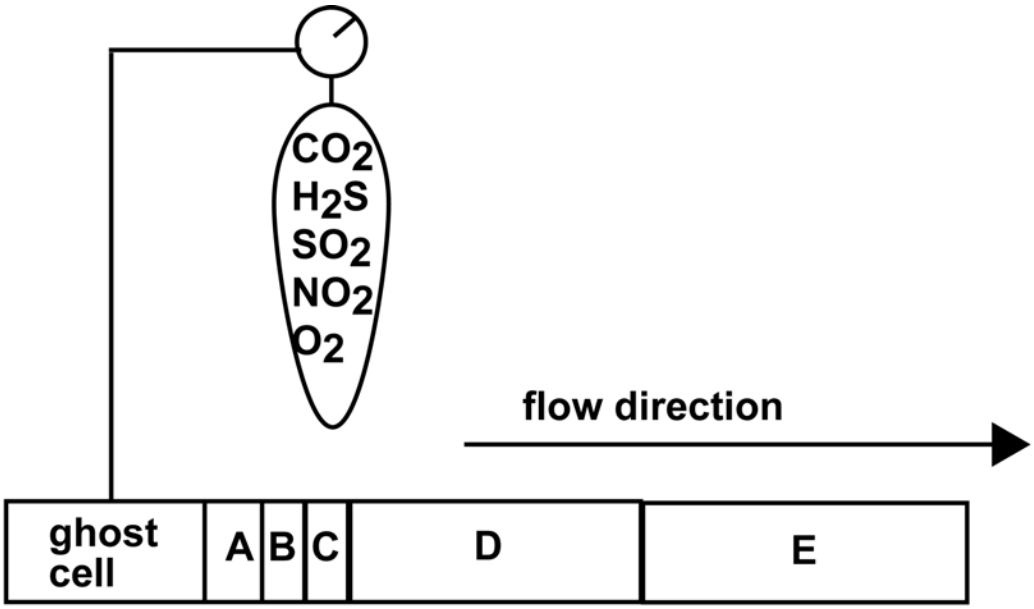

ghost cell:
formation fluid
CO_2 = 84.3b
O_2 ~ 10^{-60}b
no minerals

A = 30 x 1 m
B = 10 x 2 m
C = 5 x 4 m
D = 52 x 5 m
E = 67 x 10 m

initial condition:
formation fluid
O_2 ~ 10^{-60}b
"equilibrate" with
Quartz
K-Feldspar
Labradorite
Illite
Calcite
Kaolinite
Clinochlore
Pyrite

FIGURE 2 - MOLAL CONCENTRATIONS AND pH THROUGHOUT THE DOMAIN AT THE END OF THE INJECTION PHASE (5Y).

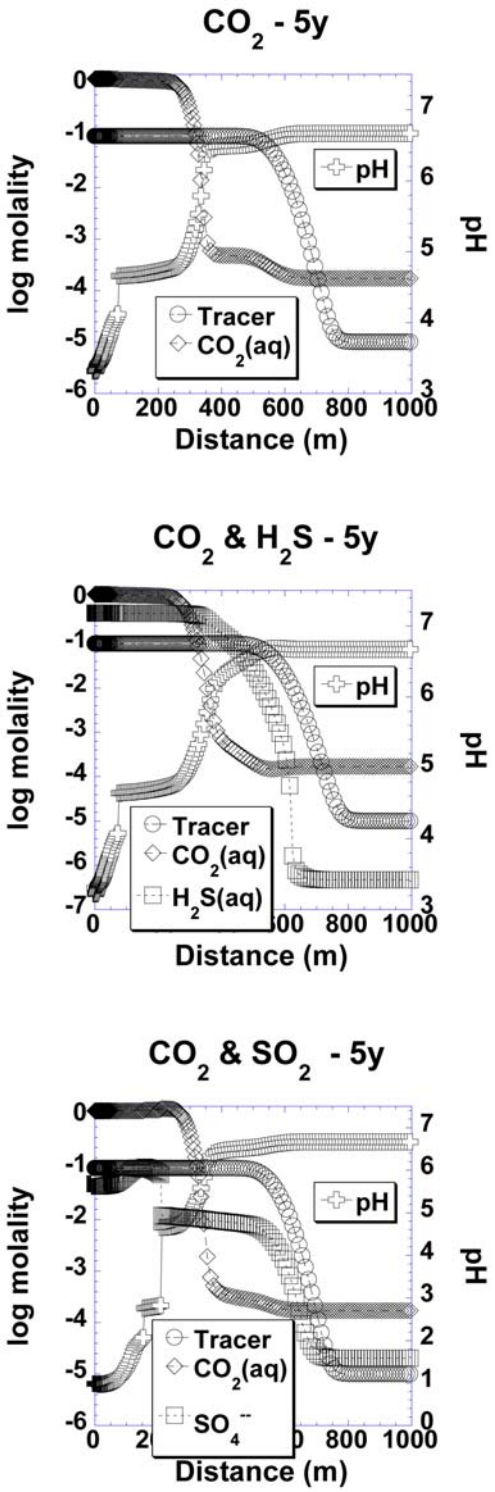

FIGURE 3 - VOLUME PERCENT OF CARBONATE MINERALS THROUGHOUT THE DOMAIN AT THE END OF THE INJECTION PHASE (5Y).

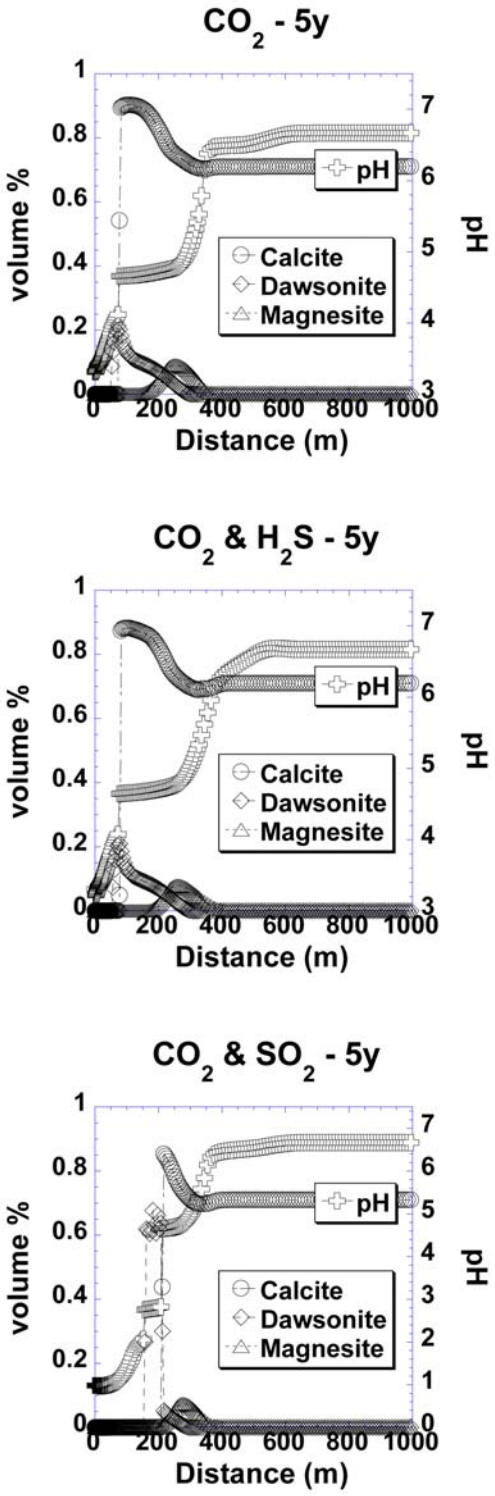

FIGURE 4 - MOLAL CONCENTRATIONS AND pH THROUGHOUT THE DOMAIN AFTER AN ADDITIONAL 95Y OF SLOW BACKGROUND FLOW.

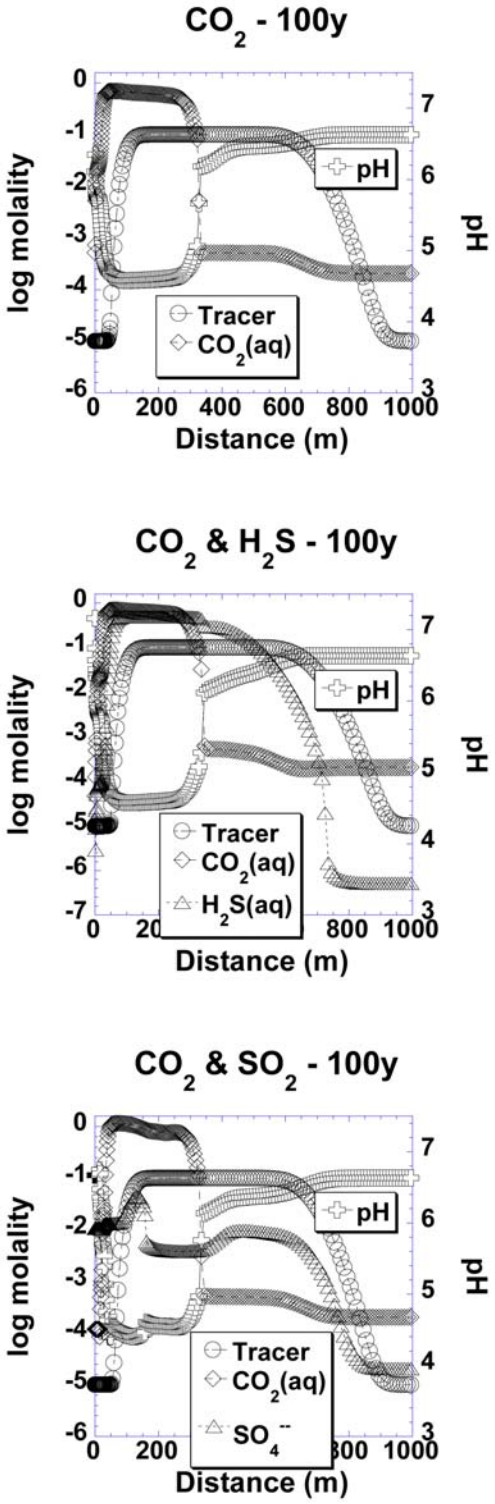

FIGURE 5 - VOLUME PERCENT OF CARBONATE MINERALS THROUGHOUT THE DOMAIN AFTER AN ADDITIONAL 95Y OF SLOW BACKGROUND FLOW.

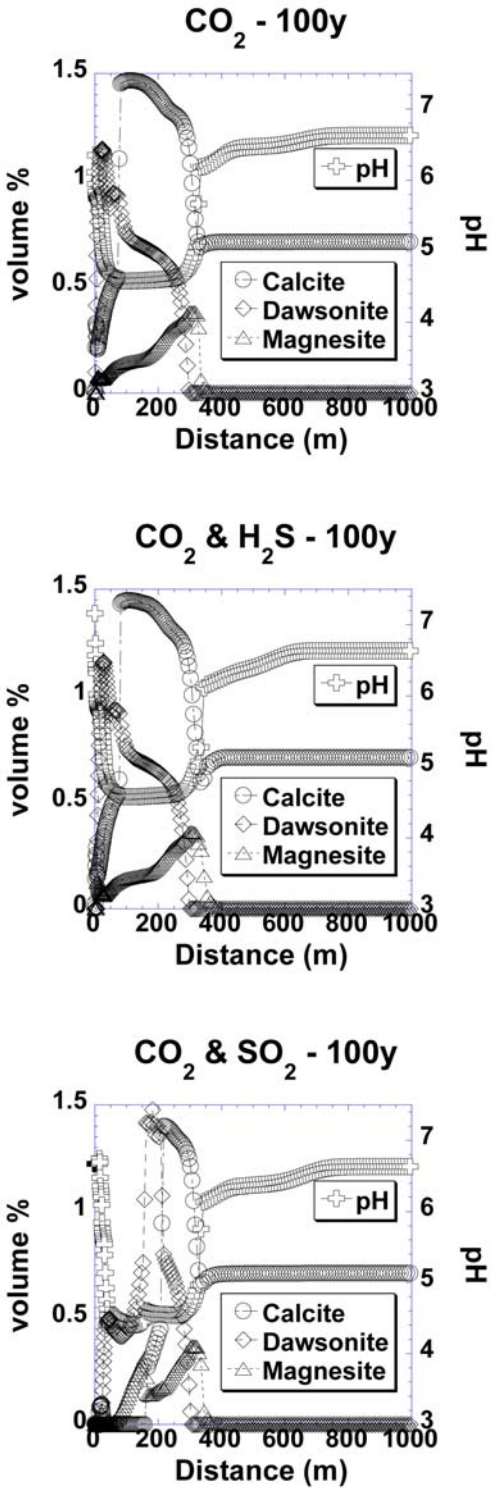

REFERENCES

Alkattan, M., Oelkers, E.H., Dandurand, J.-L. and Schott, J., 1998. An experimental study of calcite and limestone dissolution rates as a function of pH from -1 to 3 and temperature from 25 to 80C. Chem. Geol., 151: 199-214.

Baker, J.C., Bai, G.P., Hamilton, P.J., Golding, S.D. and Keene, J.B., 1995. Continental-scale magmatic carbon dioxide seepage recorded by dawsonite in the Bowen-Gunnedah-Sydney Basin system, Eastern Australia. J. Sed. Res, A65(3): 522-530.

Barton, A.F.M. and Wilde, N.M., 1971. Dissolution rates of polycrystalline samples of gypsum and orthorhombic forms of calcium sulphate by a rotating disk method. Trans. Faraday Society, 66: 764-768.

Blum, A.E. and Stillings, L.L., 1995. Feldspar dissolution kinetics. In: A.F. White and S.L. Brantley (Editors), Chemical weathering rates of silicate minerals. MIneralogical Society of America, Washington, D. C., pp. 291-351.

Chesworth, W., 1971. Laboratory synthesis of dawsonite and its natural occurrences. Nature Physical Science, 231: 40-41.

Chou, L., Garrels, R.M. and Wollast, R., 1989. Comparative study of the kinetics and mechanisms of dissolution of carbonate minerals. Chem. Geol., 78: 269-282.

Czernichowski-Lauriol, I., Rochelle, C., Lindeberg, E., Bateman, L. and Sanjuan, B., 1996. Analysis of the geochemical aspects of the underground disposal of CO_2. In: J.A. Apps and C.F. Tsang (Editors), Deep Injection Disposal of Hazardous and Industrial Waste: Scientific and Engineering Aspects. Academic Press, pp. 565-585.

Doughty, C., 2002. personal communication.

Dove, P.M. and Czank, C.A., 1995. Crystal-Chemical Controls on the Dissolution Kinetics of the Isostructural Sulfates - Celestite, Anglesite, and Barite. Geochim Cosmochim Acta 59(10): 1907-1915.

Dzombak, D.A. and Morel, F.M.M., 1990. Surface Complexation Modeling. John Wiley & Sons, New York.

Ferrante, M.J., Stuve, J.M. and Richardson, D.W., 1976. Thermodynamic data for synthetic dawsonite. Report of Investigations 8129, Bureau of Mines.

Gautelier, M., Oelkers, E.H. and Schott, J., 1999. An experimental study of dolomite dissolution rates as a function of pH from -0.5 to 5 and temperature from 25 to 80°C. Chem. Geol., 157: 13-26.

Goldbery, R. and Loughnan, F.C., 1970. Dawsonite and nordstrandite in the Permian Berry Formation of the Sydney Basin, New South Wales. Am. Mineralogist, 55: 477-490.

Goldbery, R. and Loughnan, F.C., 1977. Dawsonite, alumohydrocalcite, nordstrandite and gorceixite in Permian marine strata of the Sydney Basin, Australia. Sedimentology, 24: 565-579.

Gunter, W.D., Perkins, E.H. and Hutcheon, I., 2000. Aquifer disposal of acid gases: modelling of water-rock reactions for trapping of acid wastes. Appl. Geochem., 15: 1085-1095.

Gunter, W.D., Wiwchar, B. and Perkins, E.H., 1997. Aquifer disposal of CO_2-rich greenhouse gases: extension of the time scale of experiment for CO_2-sequestering reactions by geochemical modeling. Mineral. and Petrol., 59: 121-140.

Helgeson, H.C. and Kirkham, D.H., 1974. Thermodynamic prediction of the behavior of aqueous electrolytes at high pressures and temperatures II: Debye:Huckel parameters for activity coefficients and partial molal properties. Am. J. Sci., 274: 1199-1261.

Hovorka, S.D., Knox, P.R., Yeh, J.S., Fouad, K. and Sakurai, S., 2002. Sequestration pilot site in the Texas Gulf Coast, USA, 2002 Geological Society of America National Meeting, Denver, CO.

Jackson, J., Huggins, C.W. and Ampian, S.G., 1972. BuMines RI 7664: Synthesis and characterization of dawsonite, U. S. Bureau of Mines.

Johnson, J.W., Knauss, K.G., Glassley, W.E., DeLoach, L.D. and Tompson, A.F.B., 1998. Reactive transport modeling of plug-flow reactor experiments: quartz and tuff dissolution at 240ºC. J. Hydrol., 209(1-4): 81-111.

Johnson, J.W., Oelkers, E.H. and Helgeson, H.C., 1992. SUPCRT92: A software package for calculating the standard molal thermodynamic properties of minerals, gases, aqueous species, and reactions from 1 to 5000 bars and 0 to 1000 ^{o}C. Computers and Geosci., 18: 899-947.

Johnson, J.W., Steefel, C.I., Nitao, J.J. and Knauss, K.G., 2000. Reactive transport modeling of subsurface CO2 sequestration: Identification of optimal target reservoirs and evaluation of performance based on geochemical, hydrologic, and structural constraints, Energex 2000, Las Vegas, NV.

Kaszuba, J.P., Janecky, D.R. and Snow, M.G., 2003. Carbon dioxide reaction processes in a model brine aquifer at 200°C and 200 bars: implications for geologic sequestration of carbon. Appl. Geochem., 18: 1065-1080.

Knauss, K.G., Johnson, J.W., Steefel, C.I. and Nitao, J.J., 2001. Evaluation of the Impact of CO_2, Aqueous Fluid, and Reservoir Rock Interactions on the Geologic Sequestration of CO_2, with Special Emphasis on Economic Implications, First National Conference on Carbon Sequestration. NETL Publications, Washington, DC.

Knauss, K.G., Steefel, C.I., Johnson, J.W. and Boram, L.H., 2002. Impact of CO_2, contaminant gas, aqueous fluid, and reservoir rock interactions on the

geologic sequestration of CO_2, 2002 Geological Society of America National Meeting, Denver, CO.

Knauss, K.G. and Wolery, T.J., 1989. Muscovite dissolution kinetics as a function of pH and time at 70°C. Geochim. Cosmochim. Acta, 53: 1493-1501.

Laidler, K.J., 1987. Chemical Kinetics. Harper & Row, New York, 531 pp.

Malmstrom, M., Banwart, S., Lewenhagen, J., Duro, L. and Bruno, J., 1996. The dissolution of biotite and chlorite at 25ºC in the near-neutral pH region. Contaminant Hydrology, 21: 201-213.

Moore, J., Adams, M., Allis, R., Lutz, S. and Rauzi, S., 2003. CO_2 mobility in natural reservoirs beneath the Colorado Plateau and Southern Rocky Mountains: An example from the Springerville-St. Johns filed, Arizona and New Mexico, Second Annual Conference on Carbon Sequestration, Alexandria, VA.

Nagy, K.L., 1995. Dissolution and precipitation kinetics of sheet silicates. In: A.F. White and S.L. Brantley (Editors), Chemical Weathering Rates of Silicate Minerals. Reviews in Mineralogy, pp. 173-233.

Nagy, K.L., Cygan, R.T., Hanchar, J.H. and Sturchio, N.C., 1999. Gibbsite growth kinetics on gibbsite, kaolinite, and muscovite substrates: Atomic force microscopy evidence for epitaxy and an assessment of reactive surface area. Geochim. Cosmochim. Acta, 63(16): 2337-2351.

Pearce, J.M. et al., 1995. Natural occurrences as analogues for the geological disposal of carbon dioxide. Energy Convers. Mgmt., 37(6-8): 1123-1128.

Pitzer, K.S., 1973. Thermodynamics of electrolytes - I. Theoretical basis and general equations. Journal of Physical Chemistry, 77: 268-277.

Pruess, K., 2002. Numerical simulation of multiphase tracer transport in fractured geothermal reservoirs. Geothermics, 31(4): 475-499.

Rimstidt, J.D. and Barnes, H.L., 1980. The kinetics of silica-water reactions. Geochimica et Cosmochimica Acta, 44(11): 1683-1699.

Sass, B., Gupta, N., Ickes, J., Bergman, P. and Byrer, C., 2000. Experimental evaluation of the chemical sequestration of carbon dioxide in deep saline formations, GHGT-5, Cairns, Australia.

Smith, J.W. and Milton, C., 1966. Dawsonite in the Green River Formation of Colorado. Econ. Geol., 61: 1029-1042.

Sonderegger, J.L., Brower, K.R. and Lefebre, V.G., 1976. A preliminary investigation of strontianite dissolution kinetics. Am. J. Sci., 276: 997-1022.

Steefel, C.I., 2001. CRUNCH, Lawrence Livermore National Laboratory.

Steefel, C.I. and MacQuarrie, K.T.B., 1996. Approaches to modeling reactive transport in porous media. In: P.C. Lichtner, C.I. Steefel and E.H. Oelkers (Editors), Reactive Transport in Porous Media, pp. 83-125.

Stevenson, J.S. and Stevenson, L.S., 1965. The petrology of dawsonite at the type locality, Montreal. Can. Mineral., 8: 249-252.

Testor, J.W., Worley, W.G., Robinson, B.A., Grigsby, C.O. and Feerer, J.L., 1994. Correlating quartz dissolution kinetics in pure water from 25 to 625°C. Geochim. Cosmochim. Acta, 58: 2407-2420.

Wolery, T.J. et al., 1990. The EQ3/6 software package for geochemical modeling: Current Status. In: D.C. Melchior and R.L. Bassett (Editors), Chemical Modeling in Aqueous Systems II. Amer. Chem. Soc. Symposium Series, pp. 104-116.